Strengthening intersubunit hydrogen bonds for enhanced stability of recombinant urate oxidase from Aspergillus flavus: Molecular simulations and experimental validation

ARTICLE *in* PHYSICAL CHEMISTRY CHEMICAL PHYSICS · FEBRUARY 2009

Impact Factor: 4.49 · DOI: 10.1039/b811496j · Source: PubMed

5 AUTHORS, INCLUDING:

Zhixia Liu
The Scripps Research Institute
10 PUBLICATIONS **209** CITATIONS
SEE PROFILE

Diannan Lu
Tsinghua University
78 PUBLICATIONS **864** CITATIONS
SEE PROFILE

Wei Chen
275 PUBLICATIONS **2,009** CITATIONS
SEE PROFILE

Zheng Liu
Tsinghua University
134 PUBLICATIONS **1,719** CITATIONS
SEE PROFILE

THE JOURNAL OF PHYSICAL CHEMISTRY B

ARTICLE

pubs.acs.org/JPCB

Strengthening the Stability of a Tunnel-Shaped Homotetramer Protein with Nanogels

Zhixia Liu,[†] Diannan Lu,[†] Ling Yin,[†] Jianmin Li,[‡] Yuanchen Cui,[†] Wei Chen,[*,‡] and Zheng Liu[*,†]

[†]Department of Chemical Engineering, Tsinghua University, Beijing 100084, China

[‡]State Key Laboratory of Pathogens and Biosecurity, Beijing Institute of Microbiology and Epidemiology, Beijing 100071, China

ABSTRACT: Urate oxidase (UOX, EC 1.7.3.3) is effective for the treatment of gout and hyperuricaemia associated with tumor lysis syndrome. The inherent poor stability of UOX to temperature, proteolysis, and acidic environments is known to limit its efficacy. Herein, we encapsulated UOX into spherical and porous nanogels with diameters of 20−40 nm via a two-step in situ polymerization in the presence of oxonic acid potassium salt, an inhibitor of UOX. The UOX nanogel retained 70% of the initial activity but showed an expanded pH spectrum from pH 6−10 to 3−10 and an extended half-life at 37 °C from 5 min to 3 h. The enhanced pH stability, thermal stability, and enzyme resistance of the UOX nanogels were also confirmed by using fluorescence spectroscopy and enzymatic digestion. A molecular dynamics simulation was performed as a way to probe the mechanism underlying the formation of UOX nanogels as well as the strengthened stability against harsh conditions. It was shown that the encapsulation into the polyacrylamide network reinforced the intersubunit hydrogen bonding, shielded the hydrolytic reaction site, and thus protected the tertiary and quaternary structure of UOX. The UOX nanogel with enhanced stability provided a stable enzyme model that enables the exploration of UOX in the diagnosis and therapy of disorders associated with altered purine metabolism.

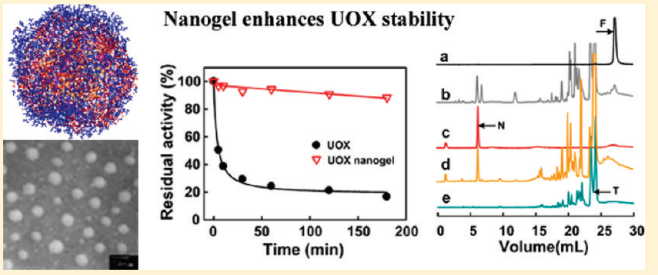

INTRODUCTION

The application of urate oxidase (uricase, UOX, EC 1.7.3.3) for the determination of uric acid in serum and urine has been pursued for the diagnosis and therapy of those disorders associated with altered purine metabolism, where elevated levels of uric acid are associated with leukemia, pneumonia, kidney injury, hypertension, and gout.[1−3] On the other hand, a reduced level of uric acid as a reducing agent indicates an inadequate protection of tissues and cells from free oxygen radicals.[3,4] The use of UOX is, however, hampered by its poor stability in dilute solution, at high temperature, in acidic pH, and from proteolysis. An enhanced stability for UOX is also beneficial for its fabrication, storage, and application in uric acid biosensors.

Besides protein engineering and addition of various solutes, chemical approaches have been proved effective for enzyme stabilization via surface modification of enzymes, immobilization on various macromolecular supports, or by forming cross-linked . Enzymes are encapsulated into various nanostructured materials, such as mesoporous silica,[7,8] nanoparticles,[9,10] and single enzyme nanocomposites.[11,12] We have previously reported single enzyme nanogels fabricated via an aqueous two-step in situ polymerization to improve enzyme stability at elevated temperature and in organic solvents. The hydrophilic polymer shells surrounding each enzyme also help to suppress protein aggregation, making single enzyme nanogels promising modules in further modification or encapsulation. This method has been applied to small proteins, such as horseradish peroxidase,[12] bovine carbonic anhydrase,[13] and lipase,[14] without compromise of enzyme activity. Its application in multisubunit proteins (oligomeric proteins), however, has not yet been attempted and limited by comprehensive encapsulation of all subunits and severe loss of enzymatic activity.

Recent years have witnessed the progress in the stabilization of UOX via immobilization on cellulose membranes, polyaniline, chitosan membranes, or sol−gel matrixes for biosensor use.[15−19] For biopharmaceutical use, UOX−polymer conjugates have been constructed applying poly(ethylene glycol), poly(*N*-vinylpyrrolidone), or poly(*N*-acryloilmorpholine).[20−22]Veronese et al.[23] have shown that the branched PEG covered a larger surface area of UOX than that by a linear PEG and thus gave enhanced biological, pharmacokinetic, and immunological properties of UOX, indicating that a high modification degree and high surface coverage favors the performance of UOX conjugates. Nevertheless, UOX is fragile to chemical modification especially at a high modification degree.[24] Our recent efforts have illustrated the significant role of intersubunit hydrogen bonding underlying the stability of UOX and suggested that strengthening of intersubunit hydrogen bonding may pave the way to higher stability of UOX.[25] The application of a single enzyme nanogel in UOX may have advantages: (1) that involvement of small molecules in the reaction

Received: September 18, 2010
Revised: April 26, 2011
Published: June 23, 2011

eliminates the steric hindrance in forming UOX−polymer conjugates and helps obtaining a high modification degree, (2) an acquisition of a UOX nanogel with a fully covered surface, (3) the multipoint linkage with the polymer network may strengthen its structural rigidity against thermal fluctuation, and (4) the presence of a hydrophilic network may shield the direct contact of UOX with the denaturing reagent, including protease.

The present study started with the encapsulation of recombinant UOX into a nanogel via an aqueous two-step in situ polymerization that was accomplished in the presence of oxonic acid potassium salt, a competitive inhibitor of UOX, to protect UOX during nanogel fabrication. The catalytic behaviors of native and encapsulated UOX were then compared at acidic pH and high temperature, together with fluorescence spectroscopy measurements. The stability against proteolysis was tested using trypsin as the model protease and characterized by reversed phase chromatography. Finally, a molecular dynamics simulation was performed to illustrate how the polyacrylamide nanogel affected the intrinsic stability of UOX and the conformational properties of fabricated UOX nanogels at elevated temperatures and against proteolysis. The results obtained in the present study indicated that the nanogel was a promising enzyme model for applications of UOX, especially in adverse conditions.

MATERIALS AND METHODS

Materials. Urate oxidase was expressed in *Escherichia coli* BL21 (DE3) by cloning the encoding region of *Aspergillus flavus* urate oxidase into pET-32a.[26] The main chemicals used in this study, including trypsin (from bovine pancreas), *N*-acryloxysuccinimide, ammonium persulfate, *N*,*N*,*N*′,*N*′-tetramethylethylenediamine, acrylamide, and *N*,*N*′-methylene bisacrylamide, were purchased from Sigma-Aldrich (St. Louis, USA). Oxonic acid potassium salt was purchased from Acros Organics (Geel, Belgium), and uric acid was purchased from Alfa Aesar (Ward Hill, USA). The Sephadex G-75 column was purchased from Amersham Biosciences (Pittsburgh, USA). The TSK-Gel G2000 SW_{XL} column was supplied by TOSOH (Tokyo, Japan). The Shim-pack VP-ODS column was purchased from SHIMADZU (Kyoto, Japan). Other chemicals were all of analytical grade.

Procedures. *Acryloylation of UOX.* UOX (36 mg) containing a given concentration of oxonic acid potassium salt was dissolved in 10 mL of pH 9.6 100 mM boric acid buffer. *N*-acryloxysuccinimide (3 mg), dissolved in 0.3 mL of DMSO, was then slowly added to the solution. The reaction was carried out at 4 °C for 4 h. Finally, unreacted molecules were removed by dialysis using a dialysis tube with a cutoff molecular weight of 12 kD against pH 7.0, 50 mM phosphate buffer.

In Situ Polymerization. A 6 mg portion of acryloylated UOX containing a given concentration of oxonic acid potassium salt was dissolved in 9 mL of pH 7.0, 50 mM phosphate buffer and purged with nitrogen. In situ radical polymerization was initiated by adding 8 mg of ammonium persulfate and 0.28 mL of *N*,*N*,*N*′,*N*′-tetramethylethylenediamine. Afterward, 420 mg of a monomer solution containing acrylamide and *N*,*N*′-methylene bisacrylamide (molar ratio = 50:1) dissolved in 1 mL of deoxygenated and deionized water was dropped into the test tube within 60 min. The reaction was continued for another 2 h at 4 °C. The unreacted proteins, monomers, and initiators were removed by gel filtration with Sephadex G-75.

Assays. *Determination of Reacted Amine Groups.* The number of unreacted amine groups on the acryloylated UOX was determined by trinitrobenzene sulfonate colorimetric assay.[27,28] Briefly, 6 μL of 2,4,6-trinitrobenzenesulfonic acid at a concentration of 2.5% (w/v) was added to 1 mL of the protein sample dissolved in pH 9.6 100 mM boric acid buffer. After incubation in the dark for 2 h at 30 °C, the absorbance of the sample was measured at 420 nm. The number of amine groups on the free UOX was also determined and used as a control.

Protein Concentration. The concentrations of free and UOX nanogel were determined using the bicinchoninic acid (BCA) protein assay kit (Beyotime, China).

Size Exclusion Chromatography. Size exclusion chromatography was performed on a TSK gel column ($G2000SW_{XL}$, Tosoh) attached to an HPLC system (Shimadzu) at room temperature. Samples were eluted with 0.1 M sodium phosphate buffer (pH 6.7) containing 0.1 M Na_2SO_4 and 0.05% NaN_3 at a flow rate of 0.5 mL·min^{-1}. The elution profiles were recorded by a fluorescence detector with an excitation wavelength of 280 nm and an emission wavelength of 330 nm.

Transmission Electron Microscopy (TEM). The TEM of the UOX/polyacrylamide mixture and UOX nanogel were determined using a Hitachi JEOL200CX high-resolution TEM. The sample, diluted in distilled water to 0.1 mg·mL^{-1}, was dropped onto the surface of carbon-coated grids. After removing the excess, 1% of pH 7.0 sodium phosphotungstate was added for negative staining.[29] The UOX nanogel sample was then exposed to air at room temperature to dry before the TEM measurement.

Fluorescence Spectroscopy. The fluorescence spectra of UOX and UOX nanogels were obtained on a Hitachi F-2500 fluorescence spectrophotometer using a quartz cuvette with a path length of 1 cm. A protein solution (0.01 mg·mL^{-1}) was excited at 280 nm, and the emission spectra were recorded from 250 to 500 nm.

Determination of UOX Activity. The activity of UOX and UOX nanogels was determined using uric acid as the substrate.[30] One unit of activity (U) is defined as the amount of UOX required to transform 1 μmol of uric acid into allantoin in 1 min at 30 °C, pH 8.9. The specific activity is the number of enzyme units per milligram of protein (U·mg^{-1}). During the assay, 30 μM uric acid was first dissolved in TEA buffer (7.5 g·L^{-1} triethanolamine, 0.38 g·L^{-1} EDTA, pH 8.9). Protein samples (0.01 mg·mL^{-1}) were then added, and the disappearance of uric acid was monitored at 292 nm on a MultiSpec-1501 spectrophotometer (Shimadzu, Japan).

The Michaelis−Menten constants for UOX and UOX nanogels were determined using uric acid as the substrate with a concentration range of 0−120 μM in TEA buffer (pH 8.9) at 37 °C. The kinetic parameters were interpreted using the Lineweaver−Burk plot.

Thermal Stability. The thermal stability of UOX and UOX nanogels were determined by incubating 0.01 mg·mL^{-1} protein samples in pH 7.0, 20 mM phosphate buffer containing 0.15 M NaCl at 37 °C. Aliquots were sampled at given time intervals and subjected to a UOX activity assay. The residual sample activity is defined as the percentage of activity remaining in the sample after incubation for a specified time versus the initial activity.

pH Stability. The pH tolerance of UOX and UOX nanogels were evaluated at 4 °C in the following buffers: 0.1 M citrate buffer (pH 3−5), 0.1 M phosphate buffer (pH 6−8), and 0.1 M boric acid buffer (pH 9−10). The 0.01 mg·mL^{-1} protein samples were incubated in the above buffers for 30 min and then subjected to UOX activity assay.

Table 1. Residual Activity of Modified UOX

		residual activity (%)
native UOX		100
1st step acryloylated UOX	no protection	44
	protected[a]	80
2nd step UOX nanogels	no protection	3
	protected[a]	70

[a] UOX was protected by oxonic acid potassium salt at a molar ratio of 1:1000.

The deactivation kinetics of UOX and UOX nanogels at pH 3 and pH 4 were evaluated by incubating the protein samples in 0.1 M citrate buffer (pH 3, 4) at 4 °C. Aliquots were sampled at given time intervals and subjected to UOX activity assay.

Proteolysis. UOX and UOX nanogels of 0.1 mg·mL^{-1} were incubated at 37 °C in pH 7.0, 20 mM phosphate buffer containing 0.15 M NaCl and 0.4 mg·mL^{-1} trypsin. Aliquots were sampled at given time intervals and subjected to UOX activity assay. Digested products were analyzed by reversed phase chromatography with a Shim-pack VP-ODS column (SHIMADZU, Japan) at a flow rate of 1.0 mL·min^{-1}. The mobile phase was composed of 0.1% trifluoroacetic acid (TFA) in water (eluent A) and 0.1% TFA in acetonitrile (eluent B). Samples were applied after equilibrating the system with 10% of eluent B. After 8 min, the acetonitrile concentration was increased with a gradient of 2.4% eluent B per minute. The elution profiles were monitored by fluorescence detection with an excitation wavelength of 280 nm and an emission wavelength of 330 nm.

Simulation. The structure of native *Aspergillus flavus* UOX was obtained from the Brookhaven Protein Data Bank (PDB code: 1R56). The GROMACS 3.3.1 package was used to perform the molecular dynamics (MD) simulation.[33] This package is a collection of programs and libraries for MD simulation and the subsequent analysis of trajectory data. Simulations were performed using the general triclinic cell geometry. Pressure and temperature coupling were implemented for all types of simulation cells. The Berendsen's weak coupling algorithm scheme was used for both pressure and temperature.

The all-atom molecular dynamic simulation was performed at pH 7 with 10 mM salt. To determine the charge distribution of UOX at pH 7.0, the internal pK_a of lysine, arginine, histidine, glutamic acid, and aspartic acid was calculated using the PCE web tool (http://bioserv.rpbs.jussieu.fr/cgi-bin/PCE-pKa)[32]. In the present study, the simple point charge model (SPC model) was used to represent the water molecule.

During the simulation, UOX was put into the center of a rectangular box using periodic boundary conditions with either water or acrylamide solution. The size of the simulation box was 28.3 × 28.3 × 28.4 nm. The system, containing one UOX molecule and a certain number of water molecules (771 681 water molecules) or a water/acrylamide mixture (194 971 water molecules/129 265 acrylamide molecules) was submitted to 500 steps of the steepest descent minimization and converged to a value of 1000 kJ·mol^{-1}·nm^{-1}, applying the particle-mesh Ewald method at different temperatures. A 10 ps position-restrained MD simulation was then performed by keeping the protein coordinate fixed and allowing the water or acrylamide molecules to equilibrate themselves. Finally, a 2000 ps MD was performed at a given temperature and a leapfrog algorithm was used for integrating the Newtonian equations of motion for 1 000 000 simulation steps, with a time step of 0.002 ps. All bonds are constrained by using LINear Constraint Solver denoted by LINCS in GROMACS.[31] For the clearness, only acrylamide and water molecules, in which the distance to UOX molecules is within 0.5 nm, are shown in figures.

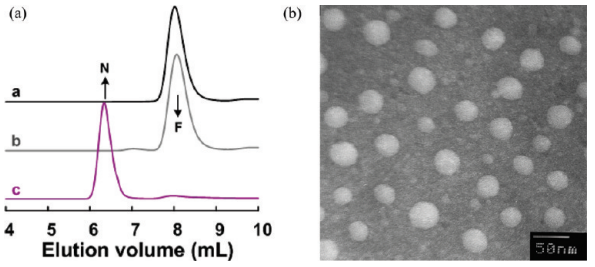

Figure 1. Characterization of UOX nanogels. (a) Elution profiles of a-UOX, b-UOX/polyacrylamide mixture, and c-UOX nanogels, in which "F" and "N" represent the elution peaks of free UOX and UOX nanogels, respectively. (b) TEM of UOX nanogels.

Herein, the root-mean-square distance (rmsd) and the number of hydrogen bonds (H bond), were used to evaluate the simulations. rmsd (Å) reflects the similarity of the specific conformation to the native one, which can be calculated by least-squares fitting the structure to the reference native structure by eq 1

$$\mathrm{rmsd}(t, t_0) = \left[\frac{1}{M}\sum_{i=1}^{N} m_i \|r_i(t) - r_i(t_0)\|^2\right]^{1/2} \quad (1)$$

where m_i is the mass of atom i in UOX, $r_i(t)$ is the internal coordinate of atom i of the conformation at time t, and $r_i(t_0)$ is the internal coordinate of atom i at the initial state, that is, the native conformation. $M = \sum_{i=1}^{N} m_i$ is the mass of UOX. A lower rmsd value of UOX indicates that its conformation is closer to that of native UOX.

Similarly, the definition of rmsd for the active site, noted as $\mathrm{rmsd}_{(A)}$ (Å), is given as follows

$$\mathrm{rmsd}_{(A)}(t, t_0) = \left[\frac{1}{M}\sum_{i=1}^{N} m_i \left\|r_i(t) - r_i(t_0)\right\|^2\right]^{1/2} \quad (2)$$

in which m_i is the mass of atom i of amino acid residues comprised by the active site, $r_i(t)$ is the internal coordinate of atom i of the conformation at time t, and $r_i(t_0)$ is the internal coordinate of atom i at the initial state, that is, the native conformation. $M = \sum_{i=1}^{N} m_i$ is the mass of all acid residues of the active site of UOX. A lower $\mathrm{rmsd}_{(A)}$ value indicates that the conformation of the active site is more similar to that of the initial one.

Hydrogen bonds were determined based on cutoffs for the angle (30°) of acceptor−donor−hydrogen and the distance of hydrogen−acceptor (0.35 nm).

RESULTS AND DISCUSSION

Preparation and Characterization of UOX Nanogels. UOX is known to be fragile to chemical modification at a high modification degree.[24] An efficient way is to apply a substrate or inhibitor into the reaction process in order to protect the active sites or prevent the key residues from being modified.[22,23] Here, the competitive inhibitor of UOX, oxonic acid potassium

Table 2. Michaelis−Menten Parameters of UOX-Catalyzed Reactions

	K_m ($\times 10^{-6}$ M)	V_{max} ($\times 10^{-3}$ M·s^{-1})	K_{cat} (s^{-1})
native UOX	13.7 ± 2.3	73.5 ± 3.3	40.0 ± 1.8
acryloylated UOX (no protection)	21.8 ± 4.7	58.6 ± 4.1	31.9 ± 2.2
acryloylated UOX (protected[a])	24.4 ± 1.4	75.4 ± 1.6	41.0 ± 0.9
UOX nanogel (no protection)	43.4 ± 9.0	10.0 ± 0.9	5.4 ± 0.5
UOX nanogel (protected[a])	37.0 ± 6.9	73.2 ± 5.5	39.8 ± 3.0

[a] UOX was protected by oxonic acid potassium salt at a molar ratio of 1:1000.

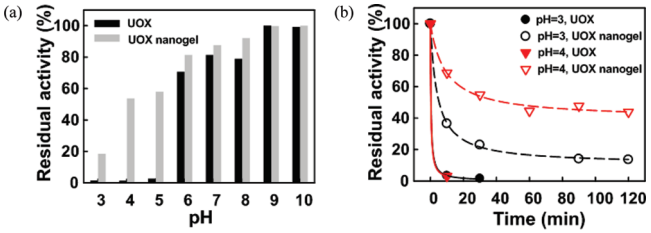

Figure 2. pH stability of native UOX and UOX nanogels. (a) Residual activity at different pH values. (b) Deactivation curves at pH 3.0 and 4.0.

salt, was applied to protect the activity of UOX while the residual activities were monitored during the synthesis.

As determined with the TNBS method detailed in the Materials and Methods section, there are 50−60 accessible amino groups on the surface of UOX and more than half of these have reacted in the first step. The residual activities of UOX after acryloylation and encapsulation were monitored and are listed in Table 1.

As shown in Table 1, in the absence of oxonic acid potassium salt, the residual activity of UOX is down to 44% after acryloylation, whereas the obtained UOX gel has almost no enzymatic activity. In the presence of oxonic acid potassium salt, the residual activity of the acryloylated UOX is 80%. After encapsulation, the residue activity of the UOX nanogel reaches 70%, which may be due to the extra hindrance to mass transfer and protein conformational transition. This demonstrates the effectiveness of oxonic acid potassium salt as a protector for those key amino groups located at the active sites of UOX.[23]

The encapsulation of UOX into nanogels was characterized by size exclusion chromatography. The size and morphology of UOX nanogels was observed using a transmission electron microscope. The results are shown in Figure 1.

In Figure 1a, a fluorescence detector is applied to eliminate the interference of UV signals generated by polyacrylamide. It is shown that the UOX nanogel is eluted earlier than both free UOX and the UOX/polyacrylamide mixture, indicating the formation of polyacrylamide-encapsulated UOX. As shown in Figure 1b, spherical nanoparticles with a diameter range of 20−40 nm are obtained via the encapsulation, which is consistent with that determined with dynamic light scattering (DLS).

Catalytic Behavior of UOX Nanogels. Table 2 gives Michaelis−Menten parameters of UOX and UOX nanogels using uric acid as the substrate.

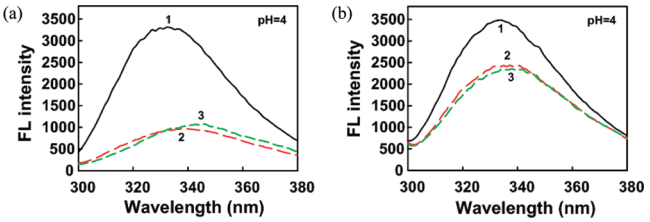

Figure 3. Fluorescence spectra change of UOX and UOX nanogels. Incubated in pH 4.0 solution for (1) 0, (2) 10, and (3) 60 min: (a) UOX and (b) UOX nanogels.

As shown in Table 2, the modification with *N*-acryloxysuccinimide leads to an increase of K_m by nearly 2-fold. This might be due to the elimination of positively charged lysine residues on the UOX surface, which impairs its attraction to the negatively charged substrate. The K_m of the UOX nanogel is increased by nearly 3-fold, as compared to their free counterpart. This may be due to additional steric hindrance by the polymer network surrounding the UOX.

For the products prepared in the absence of protection, K_{cat} values for both acryloylated UOX and UOX nanogels are greatly declined compared with that of native UOX. However, it is interesting to note that the K_{cat} values for both acryloylated UOX and UOX nanogels fabricated in the presence of oxonic acid potassium salt remain essentially the same as that of its native counterpart, meaning that the UOX nanogel maintains the catalytic efficiency of their native counterpart. On the other hand, this demonstrated the effectiveness of the oxonic acid potassium salt in protecting the active sites of UOX. For the following section, unless stated otherwise, only the UOX nanogels fabricated in the presence of site protection were used in the experimental study.

pH Tolerance of Free UOX and UOX Nanogels. Figure 2a gives the residual activity of free UOX and UOX nanogels at different pHs after 30 min incubation at 4 °C, whereas Figure 2b specifies the deactivation kinetics at acidic buffers. The protein concentration was 0.01 mg·mL^{-1} in the experiments.

As shown in Figure 2a, the native UOX loses almost all its activity after 30 min incubation at pH 3−5, whereas the UOX nanogel maintains 20−60% of the initial activity. Moreover, Figure 2b shows that the native UOX loses all its initial activity within the first 10 min, whereas the UOX nanogels maintain 20% and 50% of activity after 2 h at pH 3.0 and 4.0, respectively. For ease of comparison, the half-life of enzyme activity ($t_{1/2}$), which is defined as the time length at which the enzyme loses half of its initial activity, is interpreted from the curves in Figure 2, where $t_{1/2}$ is nearly zero for native UOX at pH 3.0 and 4.0 and is 5 and 40 min for the UOX nanogels at pH 3.0 and 4.0, respectively.

Figure 3 monitors the changes of the fluorescence spectra for native UOX and UOX nanogels at pH 4.0. During the experiment, the concentration of UOX was maintained at 0.01 mg·mL^{-1}; aliquots were taken at the given time intervals and measured immediately.

As shown in Figure 3a, the native UOX gives a maximum emission at 330 nm at the beginning of the measurement. This emission peak position is shifted to 340 nm when being placed in an acidic environment (pH 4.0) along with a dramatic reduction of the emission intensity. The significant changes in the emission suggest changes in the tertiary conformation of the native UOX. On the contrary, only minor changes in both peak position and

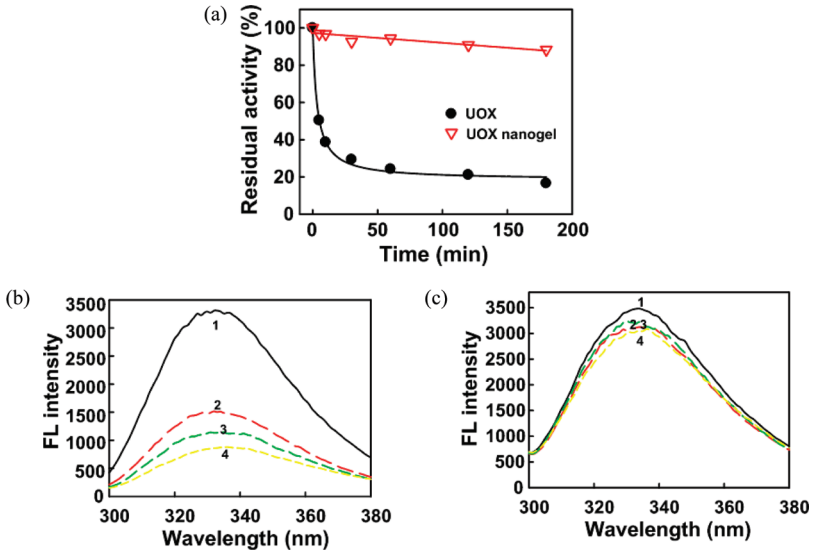

Figure 4. Stability and structural changes of UOX and UOX nanogels at 37 °C. (a) Deactivation kinetics curves. (b, c) Fluorescence spectra of UOX and UOX nanogels, respectively, incubated at 37 °C for (1) 0, (2) 5, (3) 60, and (4) 180 min.

fluorescence intensity occurs in the UOX nanogel, as shown by Figure 3b. This indicates that the polymeric network has strengthened the structural integrity of the protein.

Thermostability of Native UOX and UOX Nanogels. An improved thermal stability for UOX may enable a longer shelf life and facilitate practical applications, and this has driven a number of studies of chemical modification methods for UOX.[15−17,22,23] The deactivation curves of the native UOX and the UOX nanogels were determined at 37 °C as follows. Samples were dissolved in pH 7.0, 20 mM phosphate buffer containing 0.15 M NaCl, giving a protein concentration of 0.01 mg·mL^{-1}. Aliquots were taken at given time intervals and subjected to an activity assay and fluorescence spectra measurement.

As shown in Figure 4a, the half-life ($t_{1/2}$) of native UOX is 5 min, whereas the UOX nanogel retained nearly 90% of its initial activity after 3 h. It also can be seen from Figure 4b that a red shift of the emission peak, initially at 330 nm, occurrs for the free UOX at 37 °C, together with a reduction of peak intensity. In contrast, the UOX nanogel maintained its peak position at 330 nm with only a minor reduction of the peak intensity over the entire test period up to 3 h, as shown in Figure 4c.

Proteolysis of Free UOX and UOX Nanogels. Proteolysis represents a particular challenge to both the diagnosis of physiological fluids and the drug delivery. Here, the resistances of UOX and UOX nanogels against proteolysis are compared using trypsin as the representative protease. According to the description in the Materials and Methods section, UOX and UOX nanogels with protein concentrations of 0.1 mg·mL^{-1} were dissolved in pH 7.0, 20 mM phosphate buffer containing 0.15 M NaCl. Trypsin was then added at a terminal concentration of 0.4 mg·mL^{-1}, and the reaction was conducted at 37 °C. Aliquots were taken at given time intervals and subjected to an activity assay and fractionation by HPLC. The results are shown in Figure 5.

As shown in Figure 5a, the free UOX loses over 80% of its initial activity within 5 min, whereas UOX maintains over 50% of its initial activity after 60 min of digestion by trypsin. Figure 5b shows the reversed phase HPLC analysis of the digestion products of UOX and UOX nanogels, in which samples were dissolved in pH

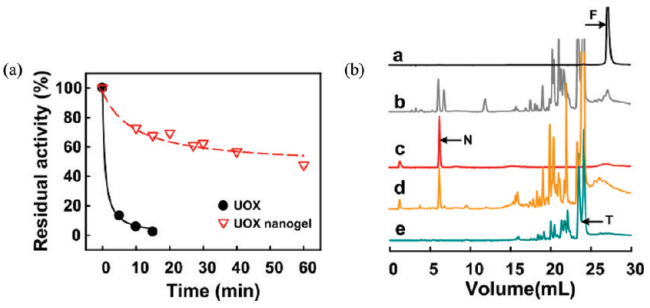

Figure 5. Proteolysis of UOX and UOX nanogels by trypsin. (a) Deactivation curves in the presence of trypsin. (b) HPLC analysis: (a) free UOX, (b) free UOX incubated with trypsin for 10 min, (c) UOX nanogels, (d) UOX nanogels incubated with trypsin for 10 min, and (e) trypsin incubated for 10 min at 37 °C. Elution peaks: "F", free UOX; "N", UOX nanogel; "T", trypsin.

7.0, 20 mM phosphate buffer containing 0.15 M NaCl and the HPLC was operated at 37 °C on a Shim-pack VP-ODS column at a flow rate of 1 mL·min^{-1} with a fluorescence detector.

As can be seen from Figure 5b, the characteristic peak of native UOX, that is, the one with an elution volume of 28 mL (curve a), almost disappears after 10 min of digestion. Instead, as shown in curve b, several small polypeptide peaks appear with elution volumes ranging from 5 to 25 mL. In contrast to the free UOX, the UOX nanogel retains its characteristic peak with an elution volume of 6 mL after trypsin digestion, as shown by curves c and d. The self-digestion of trypsin, as shown in curve e, leads to peptide peaks appearing at an elution volume of 16−25 mL; these also appear in curves b−d.

In addition, free UOX is obtained at an elution volume of 28 mL where B% reaches about 55%, whereas the UOX nanogel is obtained at 6 mL as a breakthrough peak. This suggests that the polyacrylamide-encapsulated UOX is much more hydrophilic than the free UOX.

Molecular Simulation of the Assembly of Acrylamide around the UOX. Using the protocols described in the Materials and Methods section, the assembly of acrylamide around UOX

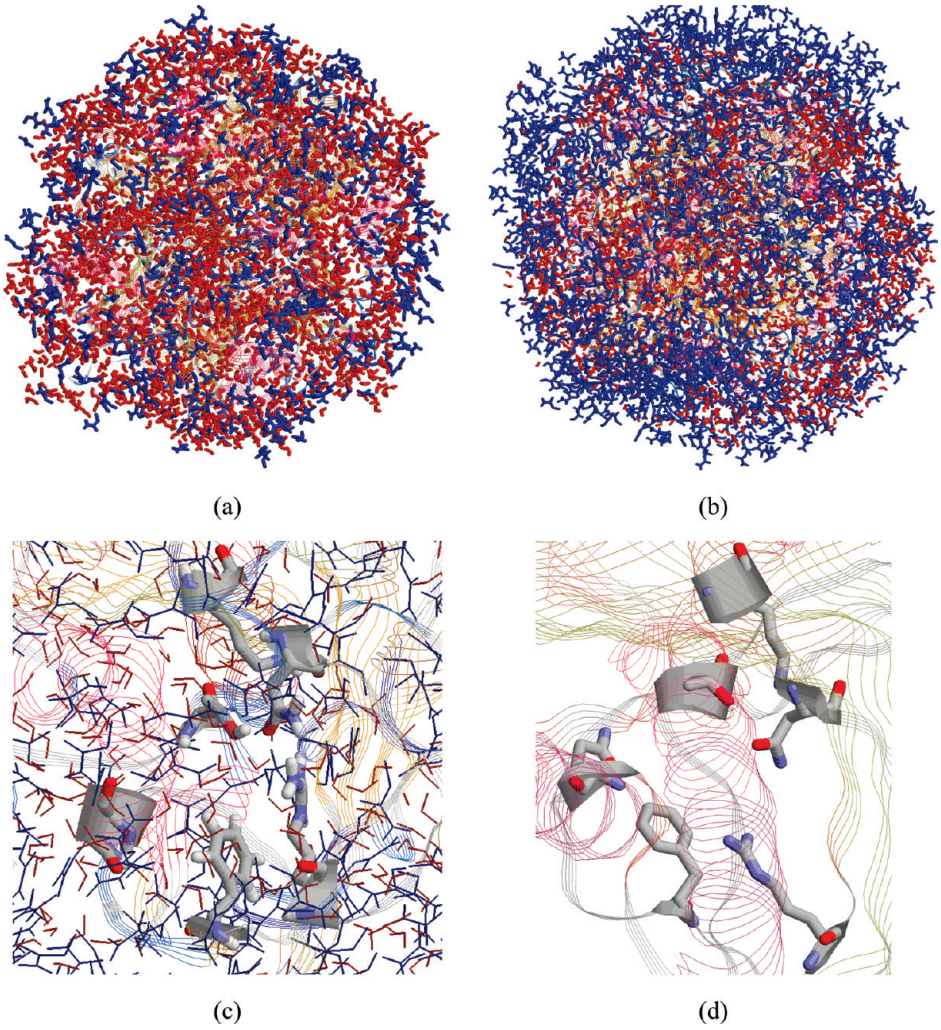

Figure 6. Molecular simulations of the UOX−acrylaimde assembly. (a) Initial state of UOX in the acrylamide/water mixture. The numbers of acrylamide and water molecules in the 0.5 nm shell around UOX are 3983 and 8544, respectively. Blue sticks: acrylamide. Red sticks: water. (b) Formation of a "core−shell" acrylamide−UOX nanogel. The numbers of acrylamide and water molecules in the 0.5 nm shell around UOX are 5082 and 5814, respectively. Blue sticks: acrylamide. Red sticks: water. (c) Active site of UOX in the UOX−acrylamide assembly. (d) Active site of the native UOX (X-ray structure).

was simulated. Figure 6 gives a representative assembly obtained at an acrylamide concentration of 40 $mg \cdot mL^{-1}$.

The initial state, as shown in Figure 6a, is characterized by an even distribution of acrylamide and water molecules around UOX. In this case, the number of molecules located within 0.5 nm of the UOX surface is 3983 and 8544 for acrylamide and water, respectively. Figure 6b gives one of the terminal assemblies after 1 ns simulation, in which the number of acrylamide increases to 5082 while the number of water molecules is down to 5814 in the 0.5 nm layer adjacent to the UOX. The enrichment of acrylamide at the surface of UOX forms the physical basis for the subsequent synthesis of UOX acrylamide nanogels, which could strengthen the structural integrity of UOX and, moreover, shield the contact between UOX and any proteolytic enzyme, as shown in Figures 3 and 5. The driving force of forming nanogels, we believe, is hydrogen bonding, as demonstrated by both simulations[14] and experiments.[33] Figure 6c shows a microscopic view of the active site of UOX in the UOX−acrylamide assembly. As compared with the native UOX shown in Figure 6d, the existence of acrylamide molecules (blue stick model) does not lead to any distortion of the active site of UOX (the difference of the rmsd of the active site of the UOX−acrylamide assembly to that of native UOX is lower than 0.1). Recalling the existence of the water molecules in the region adjacent to the UOX (Figure 6b), which is necessary for the degradation of uric acid to 5-hydroxyisourate, we suggest that the matrix of the acrylamide nanogel could strengthen the structure of UOX while maintaining essential water for UOX.

rmsd and Intrahydrogen Bonds of UOX in Free and Encapsulated Forms. As described in the Simulation section, two parameters, the root-mean-square distance (rmsd) and the number of intramolecular hydrogen bonds (intra-Hbond) for the native and encapsulated UOX at 37 °C were calculated as an index of the enhanced stability of UOX in the free or encapsulated form. The results shown in Figure 7 were generated as the average of the last 500 ps of the 2 ns simulation.

As shown in Figure 7a, the UOX nanogel has a significantly lower rmsd than the free UOX, indicating that the polyacrylamide nanogel effectively confines the thermal fluctuation and thus gives a stabilized UOX. Figure 2b shows another outcome of

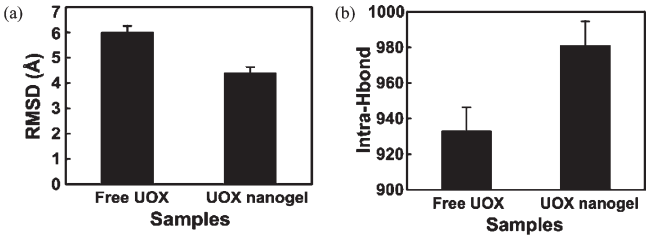

Figure 7. Conformational parameters of UOX in nanogels and solution at 37 °C: (a) rmsd (Å) and (b) number of intramolecular H bonds for free UOX and UOX nanogels.

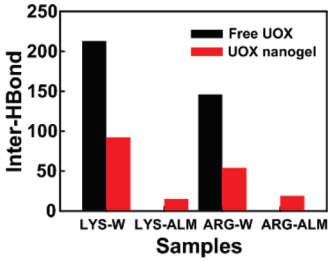

Figure 8. Interaction of lysine/arginine with surrounding solvent molecules. LYS/ARG-W represents the H-bond numbers between lysine/arginine and water; LYS/ARG-ALM represents the H-bond numbers between lysine/arginine and acrylamide.

the encapsulation, that is, an increased number of the intrasubunit H-bonds. This, as discussed elsewhere,[25] will strengthen the structural integrity of the UOX that is composed by four subunits, in addition to the reinforcement via a multipoint linkage with the porous acrylamide network. The enhanced thermal stability, as shown in Figure 7a, which is consistent with the experimental observation in Figure 4c, was attributed to the covalent linkage with the polyacrylamide gel network, which helps to strengthen the intrasubunit hydrogen bonding of UOX, as shown in Figure 7b.

Interaction of Lysine/Arginine of UOX with Solvent Molecules. To investigate the mechanism of UOX against proteolysis, as shown in Figure 5, the interaction between hydrolysis sites of UOX and test molecules (water molecules) was simulated. Here, trypsin was chosen as the representative protease, which normally cleaves peptide chains at the carboxyl side of amino acids, such as lysine and arginine. Thus, the interaction of lysine/arginine with the surrounding water or acrylamide, denoted by the number of hydrogen bonds between the lysine/arginine residue and water/acrylamide, was simulated and is summarized in Figure 8.

As shown in Figure 8, the UOX nanogel gives a significantly reduced level of H-bonding between lysine/arginine and water in comparison with free UOX. This, according to the above discussion, indicates a reduced probability of proteolysis. Instead, hydrogen bonds are formed between lysine/arginine and acrylamide; that is, the hydrolytic reaction sites are shielded by the polyacrylamide network. Therefore, the better covering of hydrolytic reaction sites by the polymeric shell around UOX is the reason for UOX nanogels against enzymatic hydrolysis.

In our previous study, the rearrangement of acrylamide around lipase has been confirmed using fluorescence resonance energy transfer (FRET), in which lipase served as a donor and pyrene as an acceptor. The variation of the emission peak property indicated the partial replacement of water molecules in the adjacent region of lipase by acrylamide due to H bonding.[14] The simulation in the present study displayed the assembly of acrylamide around UOX, as driven by H bonding, which is consistent with our previous work.[14] Subsequent polymerization with the acrylolated UOX as the cross-linker leads to a polyacrylamide network around UOX, which enhances the stability of UOX nanogels against high temperature and proteolysis.

CONCLUSION

Encapsulation of tetrameric UOX into polyacrylamide nanogels with diameters ranging from 20 to 40 nm was accomplished by an aqueous two-step in situ polymerization in the presence of oxonic acid potassium salt to protect the active sites of UOX located at subunit−subunit interfaces. Compared with free UOX, the UOX nanogel maintains essentially an identical catalytic efficiency but displays a greatly enhanced stability against acidic pH, elevated temperature, and proteolysis by trypsin. To probe the mechanism underlying the formation of UOX nanogels and the enhancement of UOX stability, an all-atom molecular dynamics simulation was performed. The molecular simulation showed the assembly of acrylamide around the UOX surface without distortion of the active sites of UOX while replacing part of the water molecules, which is the basis for both nanogel synthesis and UOX stabilization. The simulation results also illustrated that the encapsulation of UOX via a covalent linkage with the acrylamide network around UOX would greatly reinforce its conformational integrity, intensify the intersubunit bonding, and shield proteolysis. All of these lead to a greatly enhanced stability against acidic pH and elevated temperature. The enhanced stability of UOX will enable the subsequent research into the application of UOX for various purposes.

AUTHOR INFORMATION

Corresponding Author

*E-mail: liuzheng@mail.tsinghua.edu.cn (Z.L.), cw789661@yahoo.com (W.C.). Tel: 86-10-6277-9876 (Z.L.), 86-10-6694-8692 (W. C.). Fax: 96-1-06277-0304 (Z.L.), 86-10-6381-5273 (W.C.).

ACKNOWLEDGMENT

The work was supported by the National Natural Science Foundation of China (project no. 20706032, key project no. 20636040) and by the Author of National Excellent Doctoral Dissertation Special Fund (project no. 200956).

REFERENCES

(1) Heptinstall, R. H. *Gout in Pathology of the Kidney*, 2nd ed.; Little Brown: Boston, MA, 1966; pp 495−497.

(2) Arellano, F.; Sacristan, J. A. *Ann. Pharmacother.* **1993**, *27*, 337–343.

(3) Malhotra, B. D.; Chaubey, A. *Sens. Actuators, B* **2003**, *91*, 117–127.

(4) Lux, O.; Naidoo, D.; Salonikas, C. *Ann. Clin. Biochem.* **1992**, *29*, 674–675.

(5) DeSantis, G.; Jones, J. B. *Curr. Opin. Biotechnol.* **1999**, *10*, 324–330.

(6) Tor, R.; Dror, Y.; Freeman, A. *Enzyme Microb. Technol.* **1989**, *11*, 306–312.

(7) Takahashi, H.; Li, B.; Sasaki, T.; Miyazaki, C.; Kajino, T.; Inagaki, S. *Microporous Mesoporous Mater.* **2001**, *44*−*45*, 755–762.
(8) Wei, Y.; Xu, J.; Feng, Q.; Dong, H.; Lin, M. *Mater. Lett.* **2000**, *44*, 6–11.
(9) Daubresse, C.; Grandfils, C.; Jerome, R.; Teyssie, P. *Colloid Polym. Sci.* **1996**, *274*, 482–489.
(10) Martins, M. B. F.; Simoes, S. I. D.; Cruz, M. E. M.; Gaspar, R. *J. Mater. Sci.: Mater. Med.* **1996**, *7*, 413–414.
(11) Kim, J.; Grate, J. W. *Nano Lett.* **2003**, *3*, 1219–1222.
(12) Yan, M.; Ge, J.; Liu, Z.; Ou Yang, P. K. *J. Am. Chem. Soc.* **2006**, *128*, 11008–11009.
(13) Yan, M.; Liu, Z. X.; Lu, D. N.; Liu, Z. *Biomacromolecules* **2007**, *8*, 560–565.
(14) Ge, J.; Lu, D. N.; Wang, J.; Yan, M.; Lu, Y. F.; Liu, Z. *J. Phys. Chem. B* **2008**, *112*, 14319–14324.
(15) Arora, K.; Sumanaa, G.; Saxena, V.; Gupta, R. K.; Gupta, S. K.; Yakhmi, J. V.; Pandey, M. K.; Chand, S.; Malhotra, B. D. *Anal. Chim. Acta* **2007**, *594*, 17–23.
(16) Kan, J. Q.; Pan, X. H.; Chen, C. *Biosens. Bioelectron.* **2004**, *19*, 1635–1640.
(17) Yao, D. C.; Vlessidis, A. G.; Evmiridis, N. P. *Anal. Chim. Acta* **2003**, *478*, 23–30.
(18) Tsai, H.-C.; Doong, R.-A. *Anal. Biochem.* **2004**, *334*, 183–192.
(19) Akyilmaz, E.; Sezginturk, M. K.; Dinckaya, E. *Talanta* **2003**, *61*, 73–79.
(20) Caliceti, P.; Schiavon, O.; Veronese, F. M. *Bioconjugate Chem.* **1999**, *10*, 638–646.
(21) Caliceti, P.; Schiavon, O.; Veronese, F. M. *Bioconjugate Chem.* **2001**, *12*, 515–522.
(22) Schiavon, O.; Caliceti, P.; Ferruti, P.; Veronese, F. M. *Farmaco* **2000**, *55*, 264–269.
(23) Veronese, F. M.; Caliceti, P.; Schiavon, O. *J. Bioact. Compat. Polym.* **1997**, *12*, 196–207.
(24) Yasuda, Y.; F., T.; Takakura, Y.; Hashida, M.; Sezaki, H. *Chem. Pharm. Bull.* **1990**, *38*, 2053–2056.
(25) Liu, Z. X.; Lu, D. N.; Li, J. M.; Chen, W.; Liu, Z. *Phys. Chem. Chem. Phys.* **2009**, *11*, 333–340.
(26) Li, J. M.; Chen, Z.; Hou, L. H.; Fan, H. Y.; Weng, S. J.; Xu, C.; Ren, J.; Li, B.; Chen, W. *Protein Expression Purif.* **2006**, *49*, 55–59.
(27) Habeeb, A. F. S. *Anal. Biochem.* **1966**, *14*, 328–336.
(28) Snyder, S. L.; P., Z. S. *Anal. Biochem.* **1975**, *64*, 284–288.
(29) Fishbein, W. N.; Engler, W. F.; Griffin, J. L.; Scurzi, W.; Bahr, G. F. *Eur. J. Biochem.* **1977**, *73*, 185–190.
(30) Legoux, R.; Delpech, B.; Dumont, X.; Guillemot, J. C.; Ramond, P.; Shire, D.; Caput, D.; Ferrara, P.; Loison, G. *J. Biol. Chem.* **1992**, *267*, 8565–8570.
(31) *GROMACS 3.3*. http://www.gromacs.org/.
(32) PCE web tool: http://bioserv.rpbs.jussieu.fr/cgi-bin/PCE-pKa.
(33) Srivastava, A.; Ghorai, S.; Bhattacharjya, A.; Bhattacharya, S. *J. Org. Chem.* **2005**, *70*, 6574–6582.